

earthquake. Therefore, it is important to maintain a quasi-continuous and dense measure of the regional strain field.

We conclude that active deformation in the New Madrid region may be as young as several tens of thousands of years old and certainly no more than a few millions of years old. This conclusion does not rely on the offset of any particular structure within the seismic zone. We thus reconcile the short recurrence interval with lack of deformation by suggesting that the New Madrid seismic zone is a relatively young feature.

## REFERENCES AND NOTES

1. A. C. Johnston and S. J. Nava, *J. Geophys. Res.* **90**, 6737 (1985).
2. L. Liu, M. D. Zoback, P. Segall, *Science* **257**, 1666 (1992).
3. An estimation of recurrence interval of the largest earthquake in a region may be made from the measured accumulation of strain energy and knowledge of the source volume with a relation between strain and seismic moment,  $\epsilon = \Sigma M/2\mu V$  [B. V. Kostrov, *Acad. Sci. USSR Izv. Phys. Solid Earth* **1**, 23 (1974)], where  $\epsilon$  is the strain tensor,  $M$  is the moment tensor,  $\mu$  is the rigidity, and  $V$  is the source volume. A recurrence interval is derived by using the geodetic strain-rate result (2). For example, taking a maximum source length of 250 km, a breadth of 80 km, a seismogenic width (that is, depth) of 20 km, and  $\mu = 3.3 \times 10^{10}$  Pa, the time required to accumulate a maximum shear strain of  $10^{-7}$  is  $\sim 400$  years. Alternatively, changing the maximum source length to 125 km (the length of the southern arm of seismicity) and the breadth to 60 km gives a recurrence interval of  $\sim 1100$  years. The difference in estimated recurrence interval is, by itself, significant justification for determining the dimensions of the volume that is currently accumulating elastic strain.
4. D. P. Russ, R. G. Stearns, D. G. Herd, *U.S. Geol. Surv. Misc. Field Stud. Map MF-985* (1978); D. P. Russ, *Geol. Soc. Am. Bull., Part 190*, 1013 (1979).
5. N. N. Ambraseys, *Earthquake Eng. Struct. Dyn.* **17**, 1 (1988).
6. K. I. Kelson, R. B. VanArsdale, G. D. Simpson, W. R. Lettis, *Seismol. Res. Lett.* **63**, 349 (1992).
7. R. T. Saucier, *Geology* **19**, 296 (1991).
8. M. Tuttle, E. Schweig, N. Barstow, *Eos* **74**, 281 (1993); M. P. Tuttle, E. S. Schweig, R. H. Lafferty III, *ibid.*, p. 438; E. S. Schweig *et al.*, *ibid.*, p. 438.
9. R. M. Hamilton and A. C. Johnston, *U.S. Geol. Surv. Circ. 1066* (1990).
10. S. F. Obermeier, *U.S. Geol. Surv. Bull.* **1832** (1988).
11. T. L. Youd, D. M. Perkins, *J. Geotech. Eng.* **104**, 433 (1978).
12. The liquefaction severity index (LSI) method is a measure of horizontal displacement caused by lateral spreading [T. L. Youd and D. M. Perkins, *ibid.*, **113**, 1374 (1987)]. At the two most widely separated sites (A and E in Figs. 1 and 2), the LSI is at least 30. Using the curves of LSI attenuation versus distance from the seismic source for the eastern United States [T. L. Youd, D. M. Perkins, W. G. Turner, in *Proceedings, 2nd U.S.-Japan Workshop on Liquefaction, Large Ground Deformation and Their Effects on Lifelines*, National Center for Earthquake Engineering Research (NCEER), Grand Island and Ithaca, NY, 26 to 29 September 1989, T. D. O'Rourke and M. Hamada, Eds. (NCEER, Buffalo, NY, 1989), pp. 438-452] results in a magnitude of about  $M = 8.0$ .
13. F. F. Pollitz and I. S. Sacks, *Bull. Seismol. Soc. Am.* **82**, 454 (1992).
14. The magnitude of slip expected from an earthquake of a particular size may be estimated from a definition of the seismic moment,  $M_0 = \mu LWu$ , and the empirical scaling relation,  $u = 10^{-5} kL$  [C. Scholz, *ibid.* **72**, 1 (1982)], where  $M_0$  = seismic

- moment,  $\mu$  = rigidity,  $W$  = width of fault rupture,  $L$  = length of fault rupture,  $u$  = average displacement, and  $k$  is a constant of  $\sim 1.0$ . Therefore, an average slip of 8 m would be expected from a rupture of  $L = 229$  km with  $W = 20$  km or  $L = 138$  km with  $W = 30$  km, each assuming that  $\mu = 3.3 \times 10^{10}$  Pa. These figures span reasonable limits for the New Madrid region (Fig. 1).
15. E. A. Luziotti *et al.*, *Seismol. Res. Lett.* **63**, 263 (1992); E. S. Schweig III *et al.*, *ibid.*, p. 285; J. L. Sexton, H. Henson Jr., P. Dial, K. Shedlock, *ibid.*, p. 297; R. B. VanArsdale *et al.*, *ibid.*, p. 309.
16. T. G. Hildenbrand and J. D. Hendricks, *U.S. Geol. Surv. Prof. Pap.*, in press.
17. J. Watterson, *Pure Appl. Geophys.* **124**, 365 (1986).
18. D. P. Russ, *U.S. Geol. Surv. Prof. Pap. 1236-H* (1982), p. 95.
19. R. B. Herrmann and J.-A. Canas, *Bull. Seismol. Soc. Am.* **68**, 1095 (1978); D. R. O'Connell, C. G. Bufe, M. D. Zoback, *U.S. Geol. Surv. Prof. Pap. 1236-D* (1982), p. 31.
20. A. A. Barka and K. Kadinski-Cade, *U.S. Geol. Surv. Open-File Rep.* **89-315** (1989), p. 67.
21. S. G. Wesnousky, *Nature* **335**, 340 (1988).
22. E. S. Schweig III and M. A. Ellis, *Seismol. Res. Lett.* **63**, 50 (1992).
23. M. A. Naylor, G. Mandl, C. H. J. Sijpesteijn, *J. Struct. Geol.* **8**, 737 (1986); J. S. Tchalenko, *Geol. Soc. Am. Bull.* **81**, 1625 (1970).
24. E. S. Schweig III and R. T. Marple, *Geology* **19**, 1025 (1991); E. S. Schweig III, R. T. Marple, Y. Li, *Seismol. Res. Lett.* **63**, 277 (1992).
25. S. G. Wesnousky, *Bull. Seismol. Soc. Am.* **80**, 1374 (1990).
26. \_\_\_\_\_ and L. M. Leffler, *ibid.* **82**, 1756 (1992); *Seismol. Res. Lett.* **63**, 343 (1992).

27. R. T. Saucier, *Geology* **17**, 103 (1989); D. T. Rodbell and E. S. Schweig III, *Bull. Seismol. Soc. Am.* **83**, 269 (1993).
28. J. F. Ni, R. A. Snay, H. C. Neugebauer, *Seismol. Res. Lett.* **63**, 49 (1992).
29. M. L. Zoback and M. D. Zoback, *Geol. Soc. Am. Abstr. Prog.* **24**, A153 (1992).
30. G. A. Bollinger and R. L. Wheeler, *U.S. Geol. Surv. Prof. Pap.* **1355** (1988).
31. B. Bender, *Bull. Seismol. Soc. Am.* **74**, 1463 (1984).
32. M. L. Zoback *et al.*, *Nature* **341**, 291 (1989).
33. The average absolute motion of the North American plate near New Madrid (latitude  $36^\circ\text{N}$ , longitude  $90^\circ\text{W}$ ) over a fixed hotspot reference frame is  $258^\circ$  for the period 0 to 3 Ma [A. E. Gripp and R. G. Gordon, *Geophys. Res. Lett.* **17**, 1109 (1990)] and  $202^\circ$  for the period 3 to 11 Ma [D. C. Engenbretson, personal communication, and derived from D. C. Engenbretson, K. P. Kelley, H. J. Cashman, M. A. Richards, *GSA Today* **2**, 93 (1992)]. The precise age of the change in motion is unknown. The 0-3-Ma motion is well constrained back to at least 3 Ma, and the 3- to 11-Ma orientation is an average over that period.
34. Z. Reches and J. Dieterich, *Tectonophysics* **95**, 111 (1983).
35. J. M. Chiu, A. C. Johnston, Y. T. Yang, *Seismol. Res. Lett.* **63**, 375 (1992).
36. We thank M. A. Tuttle for sharing her expertise and results and D. C. Engenbretson for calculating plate motions and for helpful discussion. R. L. Wheeler, A. C. Johnston, and R. B. VanArsdale provided thoughtful reviews. Center for Earthquake Research and Information (CERI) contribution no. 187.

28 December 1993; accepted 13 April 1994

## Mechanism of Catalytic Oxygenation of Alkanes by Halogenated Iron Porphyrins

Mark W. Grinstaff, Michael G. Hill, Jay A. Labinger,\*  
Harry B. Gray\*

Halogenation of an iron porphyrin causes severe saddling of the macrocyclic structure and a large positive shift in the iron(III)/(II) redox couple. Although perhalogenated iron(II) porphyrins such as  $\text{Fe}(\text{TFPPBr}_8)$  [ $\text{H}_2\text{TFPPBr}_8$ ,  $\beta$ -octabromo-tetrakis(pentafluorophenyl)-porphyrin] are relatively resistant to autoxidation, they rapidly reduce alkyl hydroperoxides. These and related reactivity studies suggest that catalysis of alkane oxygenation by  $\text{Fe}(\text{TFPPBr}_8)\text{Cl}$  occurs through a radical-chain mechanism in which the radicals are generated by oxidation and reduction of alkyl hydroperoxides.

Iron complexes of halogenated porphyrins, such as 2,3,7,8,12,13,17,18-octabromo-5,10,15,20-tetrakis(pentafluorophenyl)porphyrinato-iron(III) chloride [ $\text{Fe}(\text{TFPPBr}_8)\text{Cl}$ ], are remarkably active catalysts for hydroxylation of light alkanes by  $\text{O}_2$ , under mild conditions ( $25^\circ$  to  $60^\circ\text{C}$ , 4 to 8 atm  $\text{O}_2$ ) (1, 2). Among the possible mechanisms considered, Lyons and Ellis have offered the suggestion that the active oxidant could be an iron-oxo intermediate,  $(\text{TFPPBr}_8)\text{Fe}^{\text{IV}}=\text{O}$ , produced through homolysis of the peroxobridged dimer formed by the reaction of  $\text{Fe}^{\text{II}}(\text{TFPPBr}_8)$  with  $\text{O}_2$

(1). Although mechanistically related to cytochrome P-450 hydroxylations (3), this system has the advantage of not requiring a co-reductant. To assess the viability of direct generation of an active hydroxylating species from  $\text{Fe}^{\text{II}}$  and  $\text{O}_2$ , we examined the electrochemical properties, reactivities, and structures of  $\text{Fe}^{\text{III/II}}(\text{TFPPBr}_8)$  complexes.

The spectroelectrochemistry of  $\text{Fe}(\text{TFPPBr}_8)\text{Cl}$  (Fig. 1) shows an isosbestic (at 457 and 580 nm) transformation between  $\text{Fe}^{\text{III}}$  (402, 442, and 560 nm) and  $\text{Fe}^{\text{II}}$  (478 and 598 nm). The high  $\text{Fe}^{\text{III/II}}$  reduction potential (0.31 V versus  $\text{AgCl}/\text{Ag}$  in 1 M KCl) suggests that  $\text{Fe}^{\text{II}}(\text{TFPPBr}_8)$  is strongly stabilized relative to other  $\text{Fe}^{\text{II}}$  porphyrins (4). Indeed,  $\text{Fe}^{\text{II}}(\text{TFPPBr}_8)$  is inert for many hours in the presence of an  $\text{O}_2$  partial pres-

Arthur Amos Noyes Laboratory, California Institute of Technology, Pasadena, CA 91125, USA.

\*To whom correspondence should be addressed.

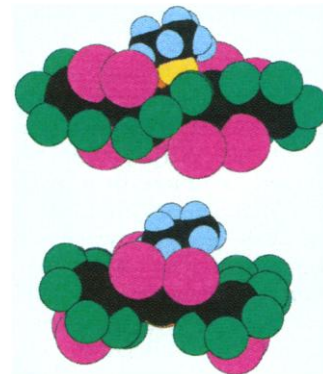
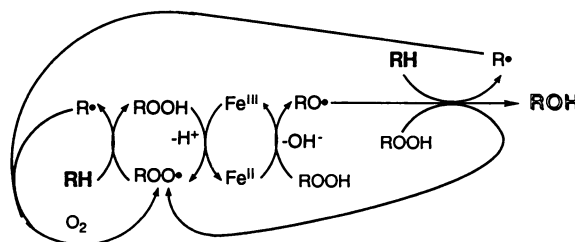
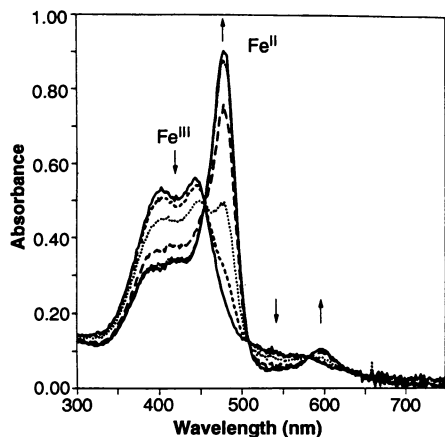


**Fig. 1 (left).** Spectroelectrochemistry of  $\text{Fe}(\text{TFPPBr}_8)\text{Cl}$  at 298 K in 0.1 M TBAH/ $\text{CH}_2\text{Cl}_2$  at an applied potential of  $\sim 0$  V versus AgCl/Ag. Arrows indicate direction of change with time. **Fig. 2 (middle).** Proposed catalytic cycle for the hydroxylation of alkanes by  $\text{Fe}(\text{TFPPBr}_8)\text{Cl}$  and  $\text{O}_2$  (1 atm) at room temperature. **Fig. 3 (right).** Space-filling molecular

models of  $\text{Fe}(\text{TFPPBr}_8)\text{OOC}(\text{CH}_3)_3$  (top, view along the pseudo- $S_4$  axis; bottom, view perpendicular to the  $S_4$  axis) show that TBHP fits in the  $\text{Fe}(\text{TFPPBr}_8)$  pocket. Color scheme: bromine, magenta; fluorine, green; oxygen, yellow; hydrogen, blue; iron, brown; and carbon, black.

**Table 1.** Selectivity of oxygenation of 3-methyl pentane. Dashes indicate none observed; spaces indicate not determined.

Fe(porph)*	Solvent	°C	Oxygen atom source	Percent yield†	Catalyst turnover‡	Alcohols			Diol	2-one	2,4-dione
						1°	2°	3°			
$\text{Fe}(\text{TFPPBr}_8)\text{Cl}$	$\text{CH}_2\text{Cl}_2$	23	PhIO	1721	25	7	4	73	—	3	13
$\text{Fe}(\text{TFPPBr}_8)\text{Cl}$	$\text{CH}_2\text{Cl}_2$	23	$\text{O}_2$ (1 atm)	192	2.2	—	—	84	—	16	—
$\text{Fe}(\text{TFPPBr}_8)\text{Cl}\S$	$\text{CH}_2\text{Cl}_2$	23	$\text{O}_2$ (1 atm)	—	—	—	—	—	—	—	—
$\text{Fe}(\text{TFPPBr}_8)\text{Cl}$	$\text{C}_6\text{H}_6$	23	$\text{O}_2$ (1 atm)	59	0.59	—	—	>99	—	—	—
$\text{Fe}(\text{TFPPBr}_8)\text{Cl}$	$\text{C}_6\text{H}_6$	60	$\text{O}_2$ (1 atm)	110	1.1	—	—	>99	—	—	—
$\text{Fe}(\text{TFPPBr}_8)\text{Cl}\ $	$\text{C}_4\text{H}_{10}$	60	$\text{O}_2$ (4.2 atm)	—	8420	—	—	91	—	—	—
$\text{Fe}(\text{TFPP})\text{Cl}$	$\text{CH}_2\text{Cl}_2$	23	PhIO	76	0.83	15	15	61	—	9	—
$\text{Fe}(\text{TFPP})\text{Cl}$	$\text{C}_6\text{H}_6$	60	$\text{O}_2$ (1 atm)	77	1.0	—	14	57	—	29	—
No porphyrin	$\text{CH}_2\text{Cl}_2$	23	PhIO	—	—	—	—	81	—	19	—
No porphyrin	$\text{CH}_2\text{Cl}_2$	23	$\text{O}_2$ (1 atm)	—	—	—	—	—	—	—	—

\*Three-hour reactions; PhIO reactions under argon; approximate molar ratios: alkane/PhIO/Fe, 7500/26/1; alkane/oxygen/Fe, 7500/10<sup>2</sup>/1. †Based on moles of Fe(porph). ‡Moles of product/moles of catalyst; ketone formation represents two turnovers. §With 0.01 M BHT. ||Oxidation of isobutane (1).

sure of 1 atm; only after more than 60 days is the spectrum of  $\text{Fe}^{\text{III}}(\text{TFPPBr}_8)\text{Cl}$  completely generated. Given this lack of reactivity, it is unlikely that an oxygenated  $\text{Fe}^{\text{II}}(\text{TFPPBr}_8)$  species ( $\text{Fe}^{\text{II}}\text{-O}_2$ ) is involved in the hydroxylation mechanism.

An iron-oxo species is a likely intermediate in  $\text{Fe}(\text{TFPPBr}_8)\text{Cl}$ - or  $\text{Fe}(\text{TFPP})\text{Cl}$ -catalyzed reactions with PhIO (Ph =  $\text{C}_6\text{H}_5$ ) as the oxidant (5). The selectivity of oxyfunctionalization of 3-methylpentane is similar for  $\text{Fe}(\text{TFPPBr}_8)\text{Cl}/\text{PhIO}$  and  $\text{Fe}(\text{TFPP})\text{Cl}/\text{PhIO}$  reactions [respectively forming tertiary (73 and 61%), secondary (4 and 15%), and primary (7 and 15%) alcohols, plus a small amount of ketones (16 and 9%)] (Table 1). In contrast, oxidation by  $\text{O}_2$  and  $\text{Fe}(\text{TFPPBr}_8)\text{Cl}$  gives higher selectivity toward the tertiary position (>99% in some cases). This discrepancy suggests that the oxidizing species in the  $\text{O}_2$  reactions is different from that in the PhIO reactions.

The most common mechanism for metal-catalyzed hydrocarbon oxidation is radical-chain autoxidation (6), in which the role of the metal is to generate radicals by

catalyzing alkyl hydroperoxide decomposition (Fig. 2). Although rapid alkane oxidation under such mild conditions (1 atm  $\text{O}_2$ , 25°C) is unprecedented, these halogenated complexes are exceptionally active catalysts for peroxide decomposition; both  $\text{Fe}^{\text{II}}(\text{TFPPBr}_8)$  and  $\text{Fe}^{\text{III}}(\text{TFPPBr}_8)\text{Cl}$  rapidly decompose *tert*-butyl hydroperoxide (TBHP) (7) (Fig. 3) (8). Computer modeling of the catalysis shows that this degree of activity would be sufficient to accelerate a radical-chain autoxidation mechanism to produce the activities and selectivities observed (9). Furthermore, inhibition by 2,6-di-*tert*-butyl-4-methylphenol (BHT), a common radical trap, was found (Table 1).

The high activity and durability of halogenated iron porphyrins as catalysts can be attributed to the following factors: (i) Electron-withdrawing substituents shift the  $\text{Fe}^{\text{III/II}}$  potential to more positive values, increasing the rate of the slow step in peroxide decomposition ( $\text{ROOH} + \text{Fe}^{\text{III}}$ ). (ii) Electronic stabilization of  $\text{Fe}^{\text{II}}$  disfavors  $\text{O}_2$  binding. (iii) Saddle-shaped structures favor monomeric porphyrin complexes

(10). (iv) Halogenation stabilizes the porphyrin against oxidative degradation (2, 4).

A superior catalyst would maintain the high reactivity of these halogenated porphyrin systems while favoring the interaction of  $\text{O}_2$  with the metal center. This situation would facilitate metal-oxo chemistry, not radical-chain autoxidation. The question of whether there are combinations of porphyrins and metals that satisfy this requirement has not yet been answered.

## REFERENCES AND NOTES

- P. E. Ellis and J. E. Lyons, *Catal. Lett.* **3**, 389 (1989); *Coord. Chem. Rev.* **105**, 181 (1990); J. E. Lyons and P. E. Ellis, *Catal. Lett.* **8**, 45 (1991); P. E. Ellis and J. E. Lyons, *J. Chem. Soc. Chem. Commun.* **1989**, 1315 (1989).
- Catalytic oxidation by metalloporphyrins (using oxidants other than  $\text{O}_2$ ) is often enhanced by halogenation of the porphyrin macrocycle [T. G. Traylor *et al.*, *J. Am. Chem. Soc.* **114**, 1308 (1992); T. G. Traylor and S. Tsuchiya, *Inorg. Chem.* **26**, 1338 (1987); P. S. Traylor *et al.*, *J. Chem. Soc. Chem. Commun.* **1984**, 279 (1984); C. K. Chang and F. Ebina, *ibid.* **1981**, 778 (1981); T. G. Traylor *et al.*, *J. Am. Chem. Soc.* **115**, 2775 (1993); H. Fujii, *ibid.*, p. 4641; T. C. Bruice and G. He, *ibid.* **113**, 2747 (1991)].

- P. Ortiz de Montellano, *Cytochrome P-450: Structure, Mechanism, and Biochemistry* (Plenum, New York, 1986); J. H. Dawson, *Science* **240**, 433 (1988).
- Cyclic voltammetric experiments on Fe(TFPPBr<sub>9</sub>)Cl and Fe(TFPP)Cl were done at 25°C under argon in CH<sub>2</sub>Cl<sub>2</sub> with 0.1 M tetrabutylammonium hexafluorophosphate (TBAH) as the supporting electrolyte. Potentials were versus AgCl/Ag in 1 M KCl. The Fe<sup>III/II</sup> couple of ferrocene was observed at 0.45 V under these experimental conditions. The Fe<sup>III/II</sup> potential of Fe(TFPPBr<sub>9</sub>)Cl is reversible when excess PF<sub>6</sub><sup>-</sup> is present. Given the similarity between these halogenated porphyrins and the chlorinated analog Fe(TPPCl<sub>9</sub>)Cl [T. Wijesekera *et al.*, *Angew. Chem.* **29**, 1028 (1990)], it is likely that the chloride remains bound or that the chloride dissociation equilibrium is faster than the rate of reduction-oxidation. The Fe<sup>III/II</sup> potential of Fe(TFPPBr<sub>9</sub>)Cl is considerably more positive than those of Fe(TFPP)Cl (-0.08 V) and Fe(TPP)Cl (-0.29 V) [L. A. Bottomley and K. M. Kadish, *Inorg. Chem.* **20**, 1348 (1981)]. Ring-centered oxidation of Fe(TFPPBr<sub>9</sub>)Cl was not observed within the solvent limit (~1.8 V), whereas oxidations of Fe(TFPP)Cl and Fe(TPP)Cl were at 1.50 and 1.30 V.
- Hydroxylation of alkanes by Fe(TFPPCl<sub>9</sub>)Cl/PhIO [J. F. Bartoli, O. Brigaud, P. Battioni, D. Mansuy, *J. Chem. Soc. Chem. Commun.* **1991**, 440 (1991); D. Mansuy, *Chem. Rev.* **125**, 129 (1993)] and Fe(TFPP)Cl/PhIO [M. J. Nappy and C. A. Tolman, *Inorg. Chem.* **24**, 4711 (1985)] has been reported.
- R. A. Sheldon and J. K. Kochi, *Metal Catalyzed Oxidations of Organic Compounds* (Academic Press, New York, 1981).
- J. E. Lyons *et al.*, *J. Catal.* **141**, 311 (1993); M. W. Grinstaff and M. G. Hill, unpublished results.
- Molecular models are based on the x-ray crystal coordinates of Fe(TFPPBr<sub>9</sub>)Cl (H. B. Gray *et al.*, in preparation) and TBHP. The extent of saddle distortion in Fe(TFPPBr<sub>9</sub>)Cl is of the same magnitude observed in Ni(TFPPBr<sub>9</sub>) [D. Mandon *et al.*, *Inorg. Chem.* **31**, 2044 (1992)]; in Cu(TFPPBr<sub>9</sub>) and Ni(TFPPBr<sub>9</sub>) [W. P. Schaefer *et al.*, *Acta Crystallogr.* **49**, 1743 (1993)]; in Cu(TFPPCl<sub>9</sub>) (W. P. Schaefer *et al.*, *ibid.*, p. 1342); in Zn(TFPPBr<sub>9</sub>) (R. E. Marsh *et al.*, *ibid.*, p. 1339); and in Zn(TPP(CH<sub>3</sub>)<sub>9</sub>) [K. M. Barkigia *et al.*, *J. Am. Chem. Soc.* **112**, 8851 (1990)].
- J. A. Labinger, *Catal. Lett.*, in press.
- Molecular models are based on the x-ray crystal coordinates of Fe(TFPPBr<sub>9</sub>)Cl (H. B. Gray *et al.*, in preparation) and Fe(TFPP)-O-Fe(TFPP) [A. Gold, K. Jayaraj, P. Doppelt, J. Fischer, R. Weiss, *Inorg. Chim. Acta* **150**, 177 (1988)]. Molecular models of Fe<sup>III</sup>(TFPPBr<sub>9</sub>)-O-Fe<sup>III</sup>(TFPPBr<sub>9</sub>) show severe steric clash between adjacent porphyrin bromine-bromine and bromine-fluorine atoms in eclipsed (along the Fe-O-Fe axis) and staggered structures, respectively.
- We thank J. E. Lyons, P. E. Ellis, W. P. Schaefer, E. R. Birnbaum, and T. Takeuchi for helpful discussions. Supported by the U.S. Department of Energy, Morgantown Energy Technology Center, and the Sun Company. M.W.G. acknowledges an NIH postdoctoral fellowship.

28 December 1993; accepted 1 April 1994

## Discovery of Intense Gamma-Ray Flashes of Atmospheric Origin

G. J. Fishman, P. N. Bhat,\* R. Mallozzi, J. M. Horack, T. Koshut, C. Kouveliotou, G. N. Pendleton, C. A. Meegan, R. B. Wilson, W. S. Paciesas, S. J. Goodman, H. J. Christian

Detectors aboard the Compton Gamma Ray Observatory have observed an unexplained terrestrial phenomenon: brief, intense flashes of gamma rays. These flashes must originate in the atmosphere at altitudes above at least 30 kilometers in order to escape atmospheric absorption and reach the orbiting detectors. At least a dozen such events have been detected over the past 2 years. The photon spectra from the events are very hard (peaking in the high-energy portion of the spectrum) and are consistent with bremsstrahlung emission from energetic (million-electron volt) electrons. The most likely origin of these high-energy electrons, although speculative at this time, is a rare type of high-altitude electrical discharge above thunderstorm regions.

We report here the detection of high-energy photons from the Earth's upper atmosphere, observed with the multiple detectors of the Burst and Transient Source Experiment (BATSE) (1) on the Compton Gamma Ray Observatory (CGRO). The

G. J. Fishman, P. N. Bhat, J. M. Horack, C. A. Meegan, R. B. Wilson, S. J. Goodman, H. J. Christian, Space Science Laboratory, NASA/Marshall Space Flight Center, Huntsville, AL 35812, USA.  
C. Kouveliotou, Universities Space Research Association, NASA/Marshall Space Flight Center, Huntsville, AL 35812, USA.  
R. Mallozzi, T. Koshut, G. N. Pendleton, W. S. Paciesas, Department of Physics, University of Alabama in Huntsville, Huntsville, AL 35899, USA.

\*Present address: Tata Institute of Fundamental Research, Bombay, 400 005 India.

apparent correlation of the events with storm systems leads us to hypothesize that they are caused by electrical discharges to the stratosphere or ionosphere. Runaway discharges to the ionosphere have been predicted (2, 3) and modeled in detail previously (4). These gamma-ray events may also be related to recently recorded optical discharge phenomena above thunderstorms (5, 6) and to other cloud-to-stratosphere discharges that have been reported in the past (7, 8).

The Compton Observatory was launched in April 1991 to perform observations of celestial gamma-ray sources. The BATSE experiment is one of four experiments on the observatory. It serves as an all-sky monitor

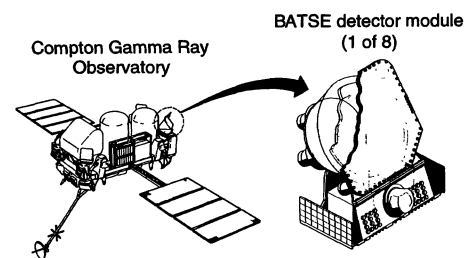


Fig. 1. The Compton Gamma Ray Observatory (CGRO). The eight BATSE detectors, with a sensitive area of about 2000 cm<sup>2</sup> each, are located on the corners of the observatory.

and has detected over 900 cosmic gamma-ray bursts, several hard x-ray transients, numerous persistent and pulsed hard x-ray sources, and several thousand solar flares. In addition, on rare occasions BATSE has recorded gamma-ray flashes from the Earth. These events have not been reported previously because it was unclear that they were real (noninstrumental) events and that they formed a distinct subclass of BATSE triggered events.

The BATSE instrument consists of an array of eight detector modules located at the corners of the observatory, arranged to provide maximum unobstructed sky coverage (Fig. 1). The scintillation detectors are sensitive to photons with energies above 20 keV. The geometry of the array ensures that sources are usually observed by four detectors. Data from the detectors are processed onboard into several data types with different temporal and spectral resolutions (1). The gamma-ray flashes reported here triggered an onboard burst data recording mode, allowing observations with high time resolution in most instances. Sources are located by comparing the relative responses of the detectors, which view different directions (9, 10).

Two features of these terrestrial events that stand out are their extremely hard spectra and their short duration. They are different from other events that have triggered the detectors, such as gamma-ray bursts, solar flares, fluctuations of other known hard x-ray and gamma-ray sources, and bremsstrahlung radiation from precipitating magnetospheric electrons. Furthermore, these events are located by the BATSE detectors as emanating from below the local horizon. The events that trigger the BATSE detectors are relatively rare, occurring less than once every 2 months. It is likely that many other weaker events of similar origin go undetected because of the trigger criteria implemented by the experiment (1, 9). Because the minimum sampling time for the triggering of the BATSE burst mode is 64 ms, the shortest of these events must be at least ~40 standard deviations above the background rate in at least two detectors to trigger the onboard system.

It is believed that prior instrumentation